Journal of
Materials Chemistry A

ROYAL SOCIETY OF CHEMISTRY

PAPER

View Article Online
View Journal

Check for updates

Cite this: DOI: 10.1039/d6ta00544f

Received 20th January 2026
Accepted 14th May 2026

DOI: 10.1039/d6ta00544f

rsc.li/materials-a

Electrically conductive MOF@carbon foam composites for atmospheric water harvesting through internal Joule heating and light irradiation

Lasse Wegner,[a] Philipp Schadte,[b] Ravi Sharma, [c] Carde Reimerdes,[a] Rainer Adelung, [bd] Joeri F. M. Denayer, [*c] Leonard Siebert [*bde] and Norbert Stock [*ad]

Atmospheric water harvesting (AWH) with microporous adsorbents shows great potential for addressing water scarcity in arid regions, but current systems face limitations due to slow sorption kinetics and high energy demands. Here, we present a proof of concept for internally heatable, hierarchically porous, conductive MOF–coated carbon foams with dynamic water adsorption capacities of up to 0.20 g g^{-1} at 40% RH. The percolating macroporous carbon foam serves as the backbone of the composites, facilitating simultaneous heat and mass transport. Regeneration of the composites is possible with mild heating at 70 °C. This can be accomplished by either solar irradiation or Joule heating, which allows for rapid desorption steps, reducing the duration of the desorption step by up to 51% compared to flushing with helium, resulting in short sorption cycles between 46 and 178 minutes. In continuous operation, the composites can potentially collect between 1.5 and 2.2 litres of water per day per kilogram of adsorbent at 40% RH.

Introduction

With rising global temperatures and a predicted growth of the human population to over 9.7 billion by 2050 (ref. 1), drinking water scarcity will be a rapidly growing challenge in the near future.[2] While coastal regions without access to fresh water can rely on desalination of seawater through reverse osmosis, landlocked arid zones need to explore other options.[3,4] Even the driest places on earth contain high amounts of water in the air that can be used for drinking and agriculture if made available. Thus, atmospheric water harvesting (AWH) has been a key technology explored scientifically since at least 1905.[5,6] There are three main approaches for harvesting water from the atmosphere.[4,5] First, reoccurring fog can be captured with meshes.[7] Unfortunately, this technique is only feasible in certain geographic locations, such as mountain ranges.[8] Alternatively water can be condensed by direct cooling of air below the dew point. Although this is possible anywhere, cooling requires high amounts of energy and is not economical in hot and dry places.[9] Lastly, water can also be harvested through adsorption using porous materials.[4,10,11] By heating the sorbent in an enclosed space, the water is desorbed and the relative humidity of the surrounding air can be increased until the water condenses and can be collected.[12] Even the driest place on earth in the Atacama desert has an average relative humidity of 17.3%.[13] Since some sorbent materials discussed for AWH can collect water at a relative humidity as low as 5%,[14] there is no limit to the regional applicability of sorbent-based AWH devices and there are already various studies showing the potential technical application of this technology.[11,15–17] The main materials that have been employed in adsorption-based AWH devices are zeolites and silica gels, which show a high affinity for water but also require energy intensive high regeneration temperatures.[18,19] Other conventional sorbents such as activated carbons do not adsorb water at low RH-values.[20] Hygroscopic salts such as $CaCl_2$ or LiCl suffer from agglomeration through deliquescence and often need to be stabilized in a matrix for long-term applications.[4,21] Metal–organic frameworks (MOFs) combine high water sorption capacities at low RH-values with mild desorption temperatures and therefore emerge as the most promising class of materials for water harvesting.[22–24] In an early design, the group of O. Yaghi developed a passive AWH device based on Zr-MOF 801 with a water harvesting capability of 0.28 L (kg d)$^{-1}$ in the Arizona desert using only solar irradiation as the mode of sorbent regeneration and thus requiring no additional input of energy.[19] Although radiative heating is a very efficient way to regenerate a sorbent since it does not require additional energy, it also limits

[a]*Institute of Inorganic Chemistry, Kiel University, Max-Eyth Straße 2, 24116 Kiel, Germany. E-mail: stock@ac.uni-kiel.de*

[b]*Functional Nanomaterials, Department of Materials Science, Kiel University, 24143 Kiel, Germany. E-mail: lesi@tf.uni-kiel.de*

[c]*Department of Chemical Engineering, Vrije Universiteit Brussel, Pleinlaan 2, 1050 Brussels, Belgium. E-mail: Joeri.Denayer@vub.be*

[d]*Kiel Nano, Surface and Interface Science (KiNSIS), Kiel University, 24118 Kiel, Germany*

[e]*Centre for Surface Chemistry and Catalysis, KU Leuven – University of Leuven, Celestijnenlaan 200F, B-3001 Leuven, Belgium*

a potential AWH device to a single sorption cycle per day.[25] This in turn requires an enormous amount of sorbent to satisfy the need for water, which is why the focus of the AWH research has shifted to actively heated devices.[23,26–29] Fortunately many of the regions that experience water scarcity also have great potential for solar energy generation.[30] This means that the energy demand for active AWH devices could be met by connecting them to solar cells while remaining independent from the local power grid.[30] In 2019, Hanikel *et al.* reported an improved prototype that used an active heating approach through electricity generated by solar cells. Employing Al-MOF-303, they achieved a water yield of 1.3 L (kg d)$^{-1}$ at 32% RH and 27 °C.[27] Even though these results are very promising, there are still three major challenges that need to be overcome for MOF-based AWH-devices on the way to become a viable technology to combat the worldwide water crisis.

(1) Energy distribution: since the thermal conductivity of MOFs is very low, it is crucial to optimize the energy distribution to ensure efficient heating and in turn short cycling times in continuous AWH operations.[31]

(2) Mass transport optimisation: the external surface area of the MOF crystals needs to be maximized to achieve short diffusion pathways, reducing cycle length further.[10,22]

(3) MOF integration: due to the fact that MOFs are usually only available as microcrystalline powders with low mechanical stability and a high pressure drop, it is important to shape the particles into monoliths or integrate them into composite materials, with the added bonus that the substrate can be used to directly deliver the heat for the sorbent regeneration.[5,12,32,33]

In this work, we present three composite materials denoted as CAU-10@CF, MOF-303@CF and MOF-801@CF. These composites are manufactured from a macroporous, framework-like carbon foam (CF) and the aforementioned MOFs. The carbon foam is structured like a connected network of beams, thus leaving a large open volume for facile water vapor transport. The inherent percolating structure of the carbon substrate combined with its electrical conductivity[34] facilitates a homogeneous and direct way of heating the surrounding MOF particles through the Joule effect, while the macropores improve the mass transport.[10] Additionally, the high photothermal conversion efficiency caused by the conjugated carbon structure allows for solar heating of the composites.[35,36] The MOFs were chosen because they each demonstrate a high water adsorption capacity over a small pressure range at low relative pressures and high stability under humid conditions.[37–39] Furthermore, both CAU-10-H and MOF-303 can be synthesized on the kg scale using green water-based synthesis procedures. This is a significant step towards industrial implementation.[40,41] A techno-economic analysis has also demonstrated the feasibility of producing CAU-10-H at a cost of around $15 per kg.[42] MOF-801 is also available through green synthesis routes, but to our knowledge, there are no reports of a kg scale synthesis so far.[43]

Experimental

Instruments

The water sorption data were collected on a DVS Advantage gravimetric sorption analyser from Surface Measurement Systems at 25 °C with nitrogen as the carrier gas and a gas flow rate of 200 sccm min^{-1}. The equilibrium criterion for considering an adsorption step as completed was a dm/dt (wt% min^{-1}) value below 0.01 for 5 min. Scanning electron micrographs were taken on a Zeiss Supra 55 VP. Sample temperatures and IR pictures were recorded using a Seek Thermal Shot infrared camera. Irradiances of the sample surfaces were measured with a S425C-L – Thermal Power Sensor Head from Thorlabs. The emission spectrum of the white light source was collected on a FLAME-T-XR1-ES spectrometer. X-ray powder diffraction (PXRD) patterns were measured on a Stoe Stadi P in transmission geometry with a MYTHEN2 1K detector using Cu-K$_{\alpha 1}$ radiation. Thermogravimetric analyses (TG) were performed on a Linseis STA PT 1000 in air with a heating rate of 4 K min^{-1}. Elemental analysis (EA) was performed with a vario MICRO cube elemental analyzer from Elementar Analysensysteme GmbH. Hydrodynamic diameters and zeta potentials of the MOF particles were measured on a Delsa™Nano C particle analyser from Beckman Coulter. Dynamic water adsorption and desorption experiments were performed under single-component vapor-phase conditions. For contacting the carbon foam (C foam) in a sealed manner, a shrink tube setup was developed. This is comprised of two 3D-printed modules between which the C foam was sandwiched. The C foam was cut into a cylindrical disk with a CO_2 laser cutter and surrounded by a fluoroethylene propylene (FEP) shrink tube provided by Reichelt Chemietechnik GmbH, Germany. Between the shrink tube and the C foam, strips of copper foil (thickness 100 μm) were placed in a quadrupole arrangement. The top and bottom modules were 3D printed with stereolithography on a Form 3B (Formlabs, USA) using Formlabs' Rigid 10K resin. The sandwiched C foam, top and bottom modules, shrink tube and copper contacts were placed into an oven at 200 °C for 2 hours until the tube was shrunk completely. During shrinking, the copper contacts were isotropically pressed against the C foam. The size between the C foam and shrink tube was varied between samples until a configuration with stable electrical contacts was found. The final diameter of the C foam disk was 25.4 mm, while the height varied but was typically 10 mm, leading to a C foam volume of ∼5 cm^3. The copper foil extended out of the shrinking tubes and could be contacted from there. A sketch of the setup can be found in Fig. S1. Glass wool was packed at both the inlet and outlet ends to ensure tight sealing. The experiments were conducted using an in-house-built breakthrough setup (Fig. S2). Breakthrough tests were carried out at relative humidities of 20% and 40% with a gas velocity of 1 cm s^{-1}. The evaporator was filled with deionized water and maintained at 35 °C, while the partial pressure of the vapour mixture was adjusted by tuning the carrier and dilution flow rates. During all experiments, the adsorption column was maintained at 298 K in a convection oven (HP 4890 GC oven). The outlet stream composition was analysed continuously using a gas chromatograph (GC, HP6890, Agilent) equipped with a Stabilwax capillary column (30 m length, 0.25 mm i.d., Restek), and FID and TCD detectors for the analysis of organics and water, respectively, using He as the carrier gas. To prevent vapour condensation, all transfer lines were heated to 70 °C. For desorption (regeneration), the copper sheet integrated in the 3D-printed module was connected to a power supply (S-LS-58, Stamos Soldering). This enabled the application of a controlled potential (0–8 V) and current monitoring (0–30 A). During regeneration, the column was continuously flushed with He, and outlet concentrations were monitored *via* GC. Prior to each experiment, the column was purged with He at room temperature for at least 60 min. Adsorption was initiated by switching to the desired H_2O vapor mixture using a multi-position valve placed upstream of the column.

Chemicals

All reagents were purchased from commercial suppliers and used without further purification.

CAU-10-H

For the synthesis of CAU-10-H with small particle sizes (hydrodynamic diameters between 200 and 700 nm), a new synthesis route was developed. For this, 80 mg (0.5 mmol) of isophthalic acid was mixed with 960 μL (0.48 mmol) of a 0.5 M solution of $Al(NO_3)_3 \cdot 9H_2O$ ($c = 0.5$ mol L^{-1}) in 2-propanol in a 4 mL glass microwave reactor. To the mixture, 720 μL of H_2O and 240 μL of 2-propanol were added, and the reactor was sealed with a Teflon cap. The synthesis was carried out under stirring at 120 °C for 6 h. After cooling to 20 °C, the product was recovered through centrifugation, washed with 10 mL of 2-propanol, water and acetone two times each, and finally dried at 90 °C overnight (yield: 78%). The final product was characterised with PXRD, EA and TG (Fig. S6, S7 and Table S1).

MOF-303

The synthesis of MOF-303 was carried out according to the literature.[27] 1.876 g (10.8 mmol) of 1-*H*-pyrazol-3,5-dicarboxylic acid monohydrate was dissolved in 181 mL of deionised water together with 6.25 mL of an aqueous solution of LiOH ($c = 2.57$ mol L^{-1}) and transferred to a screw capped jar. The solution was kept at 120 °C for 30 min, and then 2.617 g (10.8 mmol) of $AlCl_3 \cdot 6H_2O$ were added to the still hot solution and dissolved with stirring and ultrasonic treatment. The slightly cloudy mixture was kept at 100 °C for 15 h to yield a white powder. The product was isolated through filtration and washed with each 20 mL of deionised water and methanol three times, respectively, and dried overnight at 90 °C with a yield of 61% (literature yield: 42%).[27] The product was then characterised with PXRD, EA and TG (SI Fig. S8, S9 and Table S2).

MOF-801

For the synthesis of MOF-801, a procedure reported by G. Zahn *et al.* was followed.[44] 120 mg (0.517 mmol) of $ZrCl_4$ were dissolved in 10 mL of water together with 180 mg (1.55 mmol) of fumaric acid and 2.07 mL of acetic acid in a Teflon-lined steel autoclave. The autoclave was sealed and transferred to an oven preheated to 120 °C. After 24 h, the reaction was stopped and the white solid was isolated by centrifugation and subsequently washed with 10 mL of water and ethanol two times each. Finally, the product was stirred in ethanol over 48 h and dried at 90 °C, and the purified MOF was obtained with a yield of 35%. The detailed characterisation of the product can be found in the SI (Fig. S10, S11 and Table S3).

Preparation of the carbon foam

The carbon foam that was used in this work was obtained by heating 20 × 20 × 20 cm cubes of the polymer foam Basotect® W from BASF within 90 min in a nitrogen atmosphere from room temperature to 1000 °C in a HT Modell 1400-M furnace from Linn High Therm. The temperature was maintained for 20 min to fully carbonize the polymer after which the product was cooled to room temperature while still under inert conditions. The foam was thoroughly washed with deionized water to remove all mineral residues that were left after the carbonization. The product was characterised by TG, elemental analysis, nitrogen sorption at 77 K and water sorption at 298 K (Fig. S12–S14).

Manufacturing of MOF@carbon foams (MOF@CF)

The general procedure used for obtaining composite materials from MOFs and carbon foams was a liquid infiltration method. Two sample geometries were used: a flat sample and a cylindrical sample for break-through (BT) measurements. For the flat composites, 100 mg of MOF particles were suspended in 20 mL of water (the characterization of the aqueous MOF dispersions can be found in Table S4) together with 10 wt% of the polysiloxane binder SILRES® MP 50 E through ultrasonic treatment with an VWR USC600D ultrasonic cleaning bath for 30 min. Afterwards, the dispersion was dropped on the carbon substrate with dimensions of 231 mm^2 × 3 mm, which was heated to 50 °C during the infiltration to accelerate evaporation of the solvent. This procedure was repeated until a loading of *ca.* 70 wt% was achieved while being careful never to exceed the free volume of the substrate during the infiltration to avoid the dispersion drying on the surface. The amounts of MOFs in the final composites were 71 wt% for CAU-10-H, 69 wt% for MOF-303 and 69 wt% for MOF-801. To verify the presence of the MOFs in the composites, XRD patterns were collected (Fig. S15–S17).

For BT measurements, cylindrical composites with a diameter of 16 mm and a length of 6 mm were produced by infiltrating dispersions containing 8 g ethanol, 1.5 g H_2O, 0.5 g water-based carbon nanotube dispersion (0.6 wt%) and 300 wt% of the respective MOF powder, leading to composites with a loading of 73 wt% (Fig. S1).

For the Joule heating experiments, the carbon foams were embedded in a 3D-printed plastic casing (ABS polymer) and connected to two electrical contacts made from copper strips using the silver conductive paste ACHESON 1415 from PLANO GmbH prior to being infiltrated with the MOF-particles (Fig. 1).

Heating experiments

For assessing the electrical power needed to heat the materials through the Joule effect, the composites were connected to a VOLTCRAFT ESP-3010 SE DC power supply. Subsequently,

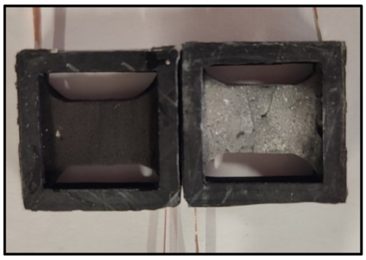

Fig. 1 Left: flat samples of pristine carbon foam with copper contacts inside the plastic casing. Right: the CAU-10-H@CF composite.

they were heated at different powers ranging from 0.25 W to 0.54 W with a fixed voltage between 4.5 and 7 V while the temperature was recorded with an IR-camera. The measurements were repeated two times each at the same power with a waiting time of 30 min between each measurement to allow for the saturation of the sample with water.

For the radiative heating, the samples were placed at varying distances to a white light source with the irradiation power on the sample surface being between 0.34 and 0.55 W. The temperature was recorded once at each distance using an IR camera with a waiting time of 30 min between two measurements of a composite at different irradiation powers.

Results and discussion

Three hierarchically porous composites composed of carbon foams coated with MOF crystals (CAU-10, MOF-303 and MOF-801) and a binder were prepared with a MOF loading between 69 and 73 wt%, and their atmospheric water harvesting behaviour under static and dynamic conditions was evaluated. To gain an understanding of the microscopic structure of the newly prepared composites, the materials were analysed by scanning electron microscopy (SEM) (Fig. 2).

The micrograph of the carbon foam (A) shows the percolating structure of the fibres, which results in a macroporous network with fibre distances of up to 100 µm. After modification with MOF dispersions, the carbon network is coated with crystallites (B–D).

The micrographs of the composites reveal that the MOF crystals cover the surface of the carbon foam closely while leaving open space between the carbon fibres. This arrangement is very advantageous because the energy transfer between the MOFs and the substrate can proceed directly without heating any extra space or relying on the poor thermal conductivity of the MOF.[31,45] Additionally, the free space of the network allows for faster gas transport through the material and maximises the exposed surface area of the MOF particles.

In the case of CAU-10@CF (B), the MOF crystallites are well dispersed on the surface of the substrate without the formation of bigger agglomerates, ensuring a good thermal contact and short diffusion pathways into the MOF crystallites. MOF-303@CF (C) shows a more inhomogeneous distribution of the MOF particles with some agglomerates of several µm forming in the macropores (C_1), while other sections show a coverage similar to CAU-10@CF (C_2). The open space around the agglomerates still allows the flow of gas through the composites

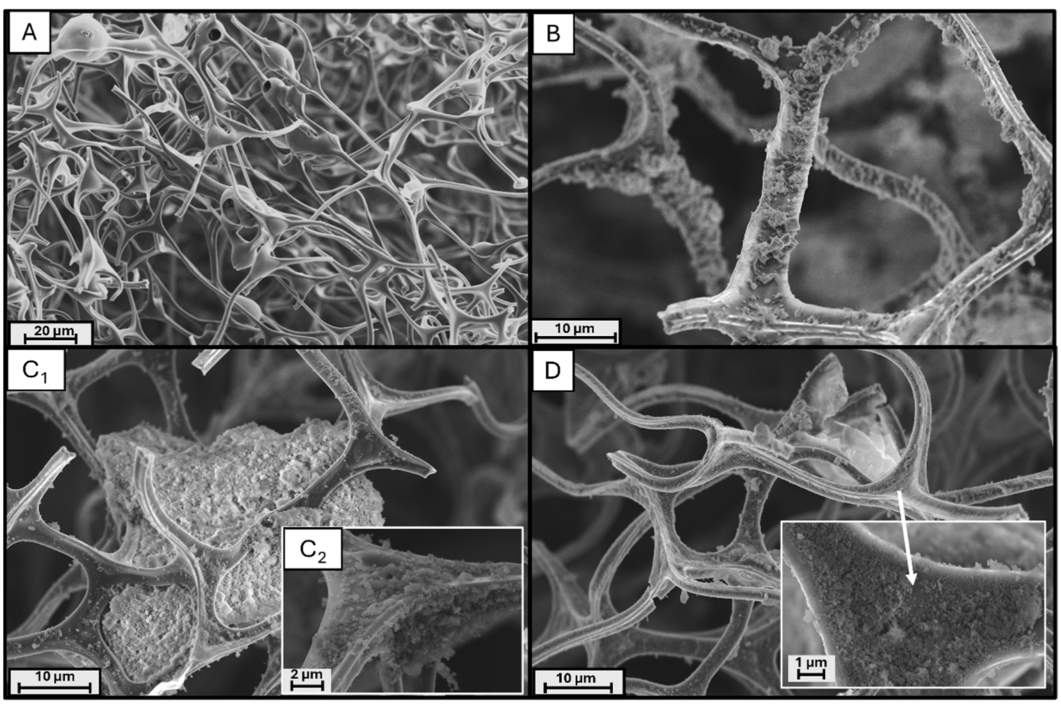

Fig. 2 Scanning electron microscopy micrographs of the unmodified carbon foam (A), CAU-10@CF (B), MOF-303@CF (C_1 and C_2) and MOF-801@CF (D). (C_1) shows a section of the composite where agglomeration of the crystallites is visible while (C_2) depicts a section with more dispersed MOF particles. The magnified section in (D) shows the close contact of the MOF-801 crystallites with the carbon fibre.

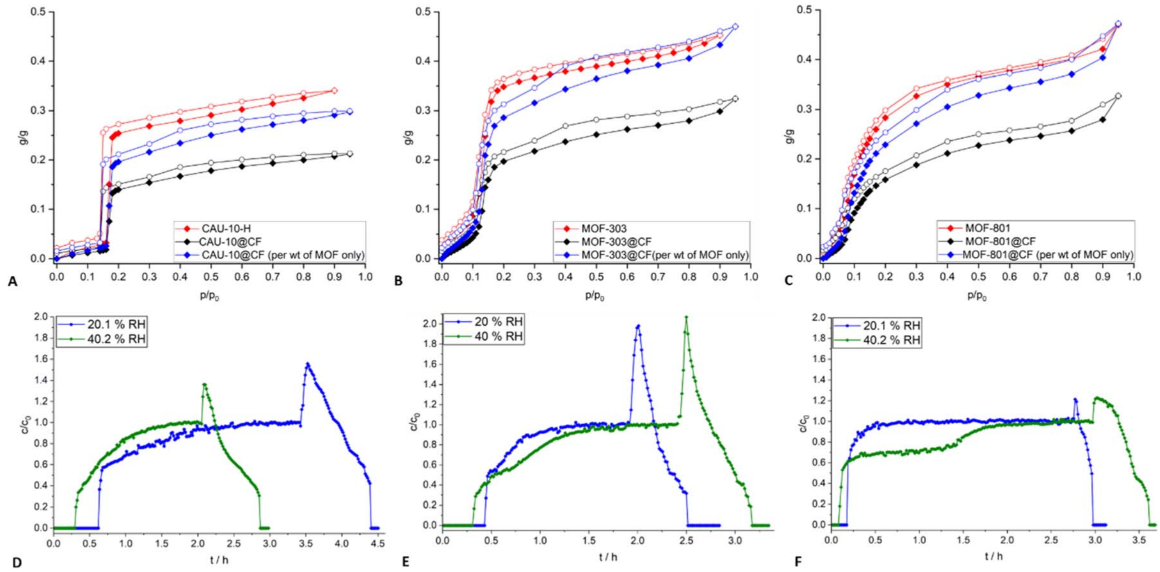

Fig. 3 (A–C) Water sorption isotherms at 25 °C for the three composite materials in comparison with the respective pristine MOF powders. All composites exhibit the desired S-shaped isotherm with reduced maximal water uptake compared to the parent MOF of 62.6% for CAU-10@CF, 71.7% for MOF-303@CF and 69.6% for MOF-801@CF. The blue curves show the calculated sorption isotherms of the composites when only the weight of the MOF is considered and the weight of the carbon substrate is ignored. The graphs below show the breakthrough measurements of the respective composites (D–F) under simulated AWH operation conditions of 20% RH (blue curves) and 40% RH (green curves) at 25 °C followed by Joule-heating assisted desorption with a heating power of 0.5 W.

Table 1 Summary of the dynamic water harvesting parameters for the three composites at 20% and 40% RH obtained from BT analysis

	RH [%]	Saturation time [min]	Desorption time [min]	Capacity [g g^{-1}]	Daily water production potential [L (kg d)$^{-1}$]
CAU-10@CF	20	119	59	0.13	1.05
CAU-10@CF	40	83	51	0.17	1.83
MOF-303@CF	20	65	37	0.14	1.98
MOF-303@CF	40	87	45	0.20	2.18
MOF-801@CF	20	29	17	0.05	1.57
MOF-801@CF	40	108	41	0.15	1.45

but the thermal contact is reduced in comparison to the other composites. MOF-801 (D) shows the most homogeneous coating of the carbon fibres, leading to high surface coverage and good thermal contact. Additionally, most MOF particles are localised directly on top of the carbon fibres, maximising the free space and heat transfer, which is a result of the smaller particle size compared to the other two MOFs (Table S4). The different behaviours of the three MOFs can be caused by their different particle sizes and zeta potentials (Table S4), leading to different interactions between the particles, the carbon substrate and the binder.[46] To analyse the sorption properties and thus the harvesting abilities of the composite materials, water sorption isotherms of the pristine MOFs and the composites were recorded at 25 °C (Fig. 3). The water sorption isotherms of the composites show a high resemblance to those of the respective MOF powders, showing that contributions from the substrate are negligible. The maximum water adsorption capacity in comparison with the parent MOF at $p/p_0 = 0.9$ is 0.21 g g^{-1} (60.8%) for CAU-10-H@CF, 0.30 g g^{-1} (66.0%) for MOF-303 and 0.28 g g^{-1} (66.4%) for MOF-801@CF, respectively. The values for MOF-303@CF and MOF-801@CF are in accordance with the expected values for the amount of MOF inside the materials, considering a negligible contribution from the carbon foam, with 95.6% of the expected capacity for MOF-303@CF and 96.0% for MOF-801@CF. In the case of CAU-10@CF, the sorption capacity equals 85.4% of the expected value, although the underlying reason remains unclear. Obvious reasons such as binder pore blocking, incomplete activation and diffusion limitations are unlikely since experimental conditions are similar to the reported ones[41] and identical for all three composites. A possible explanation could lie in sample preparation since CAU-10 forms larger particles that might lead to weaker adhesion and thus loss of material when cutting the composite into smaller pieces for the gravimetric

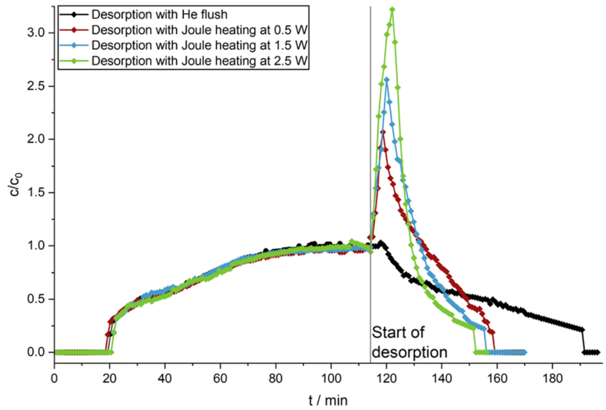

Fig. 4 Comparison of the water desorption behaviour in MOF-303@CF when activating by flushing the sample with helium and by Joule heating at different electrical power inputs. The measurement was conducted at 25 °C with a flow rate of 110 sccm and a gas velocity of 0.01 m s^{-1}. The vertical grey line shows the start of the desorption step.

sorption analysis. To assess adsorption performance under dynamic conditions, breakthrough (BT) experiments under simulated water harvesting conditions were conducted (Fig. 3).

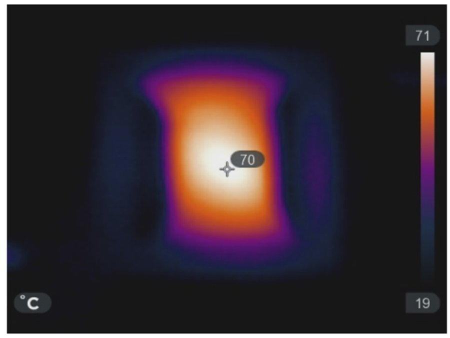

Fig. 6 Infrared photograph of the structured carbon foam heated to 70 °C through the Joule effect.

The durations of the adsorption and desorption steps as well as the water capture capacity extracted from the BT experiments are summarized in Table 1. Regarding the water capture capacity per cycle, MOF-303@CF exhibits the highest at both 20% RH as well as 40% RH with 0.14 g g^{-1} and 0.20 g g^{-1}, respectively, matching the relative performance in the static sorption experiments. Combined with its short total cycle times of 102 min at 20% RH and 122 min at 40% RH, it also exhibits

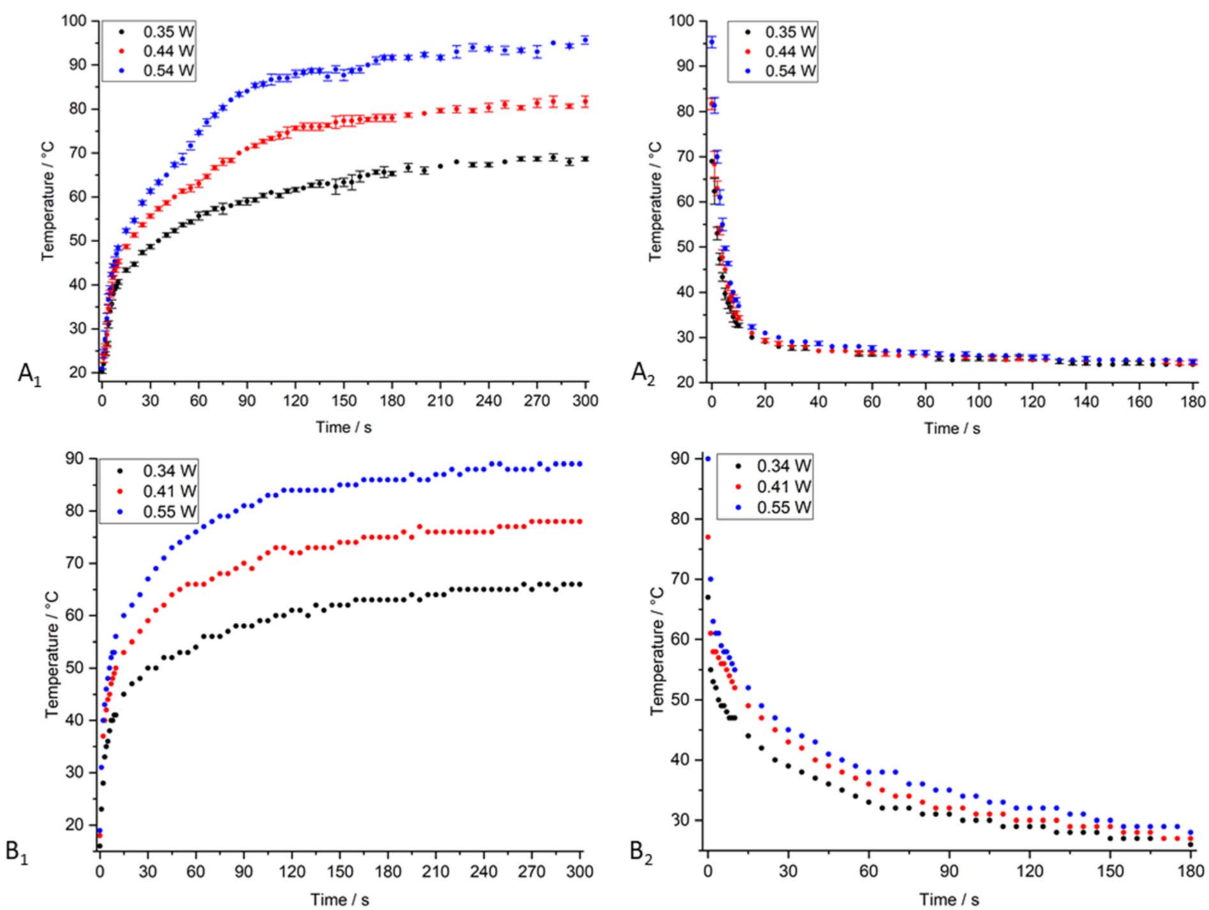

Fig. 5 Comparison of the two heating modes for the composite MOF-801@CF. (A_1 and A_2) The temperature response of the material as a function of time for Joule heating with a direct current, starting from the composite saturated with water under ambient conditions. (A_1) shows the heating behaviour after the current is applied while (A_2) depicts the cooling as a function of time after the power is turned off. (B_1 and B_2) The temperature changes for the radiative heating at different irradiances with a white light source. The heating and cooling are presented in (B_1) and (B_2) respectively. The optimal desorption temperature of 70 °C is reached after 85 s at 0.44 W with Joule heating and after 90 s at 0.41 W with radiative heating.

Table 2 Calculated energy demand for heating the composites to 70 °C *via* Joule or solar heating

P to reach 70 °C	CAU-10@CF [kW kg^{-1}]	MOF-303@CF [kW kg^{-1}]	MOF-801@CF [kW kg^{-1}]
Joule heating	9.1 ± 0.3	11.2 ± 0.8	9.3 ± 0.1
Solar heating	10.2 ± 2.9	11.0 ± 5.6	9.4 ± 4.0

the highest possible daily water production capacity with 1.98 L (kg d)$^{-1}$ and 2.18 L (kg d)$^{-1}$, respectively. At 20% RH, MOF-801 exhibits the second-best performance with 1.57 L (kg d)$^{-1}$, while CAU-10 performs better than MOF-801 at 40% RH with 1.83 L (kg d)$^{-1}$ of production capacity. All reported water production capacities are normalized to the total composite mass. A comparison with the water harvesting capacities obtained in other studies can be found in Table S6.

Three different methods for the adsorbent regeneration were investigated: Joule heating, solar irradiation and flushing with helium. Joule heating leads to the highest water production capacities, since it allows the most sorption cycles to be completed in a day, but also requires the most energy. Flushing with helium also allows multiple daily sorption cycles, but without heating, the desorption takes longer. Passive water harvesting with concentrated sunlight requires no energy input but is therefore limited to one adsorption cycle per day, using the night for adsorption and the day for desorption. Thus, the water production capacity in the solar driven AWH mode is equal to the equilibrium water uptake of the composites, which is 0.17 g g^{-1} for CAU-10@CF, 0.20 g g^{-1} for MOF-303@CF and 0.15 g g^{-1} for MOF-801@CF at 40% RH, respectively.

To investigate the influence of the regeneration process on the desorption time, Joule heating experiments at different electrical powers from 0 W to 2.5 W were conducted for MOF-303@CF, with a He gas stream of 40% RH (Fig. 4). Even at the lowest employed heating power of 0.5 W, Joule heating leads to a significant reduction in the time of the desorption step compared to just flushing the composite with the carrier gas with a reduction of 42%, from 77 min to 45 min.

Further increasing the heating power only leads to minimal improvements by decreasing the duration of the desorption step by an additional 3 minutes (4%) to 42 minutes at 1.5 W at the cost of 280% higher energy consumption and by 7 minutes (9%) down to 38 minutes at 2.5 W, increasing the energy consumption by 422%. This comparison demonstrates that the use of higher power for Joule heating is highly inefficient. To show that the composites can retain their water harvesting capacities after several Joule heating runs, the water uptake of MOF-303@CF for five BT-cycles was compared, showing no signs of degradation (Fig. S5).

From the dynamic water sorption capacities and the durations of the sorption cycles, it is possible to estimate the power consumption necessary for the desorption of water from the composites, which is between 14.8 kWh $L_{H_2O}{}^{-1}$ and 39.6 kWh $L_{H_2O}{}^{-1}$ (Table S5). Due to the small size of the reported devices and the accompanying systemic losses, the reported energy consumption has to be seen as an upper bound.

For a perfect system, the energy required for the desorption of water from the composites has been estimated to be around 1 kWh $L_{H_2O}{}^{-1}$ (Section S9). For the actual production of liquid water, additional energy requirements for the condensation unit need to be considered. Beside the sorption performance, the thermal desorption behaviour is an important parameter of an AWH device. Thus, the temperature response of flat samples of the three composites under different heating conditions, using Joule heating as well as irradiation with a white light source (Fig. S18), was investigated. The percolating nature of the electrically conductive[34] carbon substrate allows for uniform and rapid Joule heating (Fig. 5) as well as cooling of the composites. Due to the fact that the middle part of the composite is narrower than the part connected to the electrodes, the resistance is highest in the middle section, resulting in localized heating with small energy losses to the casing (Fig. 6).

The heating curves in Fig. 5 show that the saturated composite MOF-801@CF can reach the desired regeneration temperature of 70 °C in under two minutes at 0.44 W heating power (5.5 V and 0.08 A). The cooling in the ambient atmosphere proceeds on a similar timescale, so that the composite reaches $T < 30$ °C in about 20 seconds.

The heating curves of the composites prepared from MOF-303 and CAU-10-H can be found in the SI (Fig. S19 and S20). Assuming linear behaviour between heating power and temperature reached, the power needed to heat the composites to 70 °C can be calculated (Fig. S21–S23). Taking the weight of the active material into consideration, the power demand is between 9.1 and 11.2 kW kg^{-1} (Table 2).

The data for radiative heating (Fig. 5B) show that light irradiation is equally efficient at heating the composites. The comparatively slower cooling rate is caused by the heating up of the sample holder through the light source, which slows the cooling of the composite. Using the same approach as before, the power required to heat the composites to 70 °C using white light equals 10.2 ± 2.9 kW kg^{-1} for CAU-10@CF, 11.0 ± 5.6 kW kg^{-1} for MOF-303@CF and 9.4 ± 4.0 kW kg^{-1} for MOF-801@CF (Section S7), which is very close to the values obtained from the Joule heating approach (Table 2). The power needed to heat the composites to 70 °C was 1700 ± 500 W m^{-2} for CAU-10@CF, 1600 ± 800 W m^{-2} for MOF-303@CF and 1600 ± 700 W m^{-2} for MOF-801@CF. With the power demand being 60–70% higher than the standard irradiation on a cloudless day, optical concentration through Fresnel lenses or mirrors could be used to run the AWH device without the need for an additional power supply.[47] Since the penetration depth of light in these kind of materials is limited, solar irradiation can only heat the surface of the composites. Thus, the height of the materials needs to be limited to around 1 cm, which was demonstrated in similar sponge like composites as the effective penetration depth to achieve effective heating with solar irradiation.[48]

Conclusions

In this work, we present a new method for the preparation of AWH composites made of macroporous carbon foams and microporous adsorbents. To demonstrate this, we manufactured composites based on three different MOFs, namely CAU-10-H, MOF-303 and MOF-801. The percolating electrically conductive structure of the composites allows rapid Joule heating of the materials, enabling short sorption cycles between 46 and 178 minutes with a reduction in the desorption time of up to 51% compared to flushing with helium. While the performance of the composites has only been evaluated using devices on the 100 mg scale, a theoretical scale up of the devices should be able to collect between 1.5 and 2.2 L of water per kg of adsorbent per day with active heating, assuming linear scalability. Concentrated solar irradiation can be used as an alternative mode of sorbent regeneration, allowing for a single daily sorption cycle with a water yield of 0.15–0.20 L $(\mathrm{kg\ d})^{-1}$ at 40% RH. Due to the fact that the main advantages of the presented composites, such as Joule heating and improved mass transport, are architecture-driven and therefore independent of the type of adsorbent used, this method of composite preparation can likely also be employed for other solid adsorbents that can be obtained with particle sizes in the submicrometer scale.

Author contributions

Lasse Wegner: conceptualization, data curation, formal analysis, investigation, methodology, visualization, validation, writing – original draft, writing – review. Philipp Schadte: resources, data curation, formal analysis, methodology. Ravi Sharma: resources, data curation, software, formal analysis, investigation, methodology, visualization, validation, writing – review. Carde Reimerdes: formal analysis, investigation. Rainer Adelung: resources, supervision. Joeri F. M. Denayer: resources, supervision, methodology, validation, writing – review. Leonard Siebert: conceptualization, funding acquisition, project administration, resources, supervision, methodology, validation, writing – review. Norbert Stock: conceptualization, funding acquisition, project administration, resources, supervision, writing – original draft, writing – review.

Conflicts of interest

There are no conflicts to declare.

Data availability

The data supporting this article have been included as part of the supplementary information (SI). Supplementary information is available. See DOI: https://doi.org/10.1039/d6ta00544f.

Acknowledgements

LS, PHS and RA gratefully acknowledge funding by the Germany Federal Ministry for Economic Affairs and Energy under the Grant No. KK5010204 MP1. LS gratefully acknowledges funding of a Walter-Benjamin Fellowship by the Deutsche Forschungsgemeinschaft (DFG, German Research Foundation) under the grant number SI 3288/1-1 708627. NS and LW acknowledge the network Water4All, within the scope of the project with reference Water4All/0003/2022.

Notes and references

1 United Nations, Department of Economic and Social Affairs, Population Division, *World Population Prospects 2022*, Online Edition, 2022.
2 UNESCO World Water Assessment Programme, Leaving no one behind, Unesco, Paris, 2019.
3 M. Qasim, M. Badrelzaman, N. N. Darwish, N. A. Darwish and N. Hilal, *Desalination*, 2019, **459**, 59–104.
4 W. Shi, W. Guan, C. Lei and G. Yu, *Angew Chem. Int. Ed. Engl.*, 2022, **61**, e202211267.
5 H. Lu, W. Shi, Y. Guo, W. Guan, C. Lei and G. Yu, *Adv. Mater.*, 2022, **34**, e2110079.
6 V. S. Nikolayev, D. Beysens, A. Gioda, I. Milimouka, E. Katiushin and J.-P. Morel, *J. Hydrol.*, 1996, **182**, 19–35.
7 S. Korkmaz and İ. A. Kariper, *Environ. Chem. Lett.*, 2020, **18**, 361–375.
8 Y. Tu, R. Wang, Y. Zhang and J. Wang, *Joule*, 2018, **2**, 1452–1475.
9 B. Gido, E. Friedler and D. M. Broday, *Atmos. Res.*, 2016, **182**, 156–162.
10 A. LaPotin, H. Kim, S. R. Rao and E. N. Wang, *Acc. Chem. Res.*, 2019, **52**, 1588–1597.
11 K. Yang, T. Pan, Q. Lei, X. Dong, Q. Cheng and Y. Han, *Environ. Sci. Technol.*, 2021, **55**, 6542–6560.
12 T. Li, M. Wu, J. Xu, R. Du, T. Yan, P. Wang, Z. Bai, R. Wang and S. Wang, *Nat. Commun.*, 2022, **13**, 6771.
13 A. Azua-Bustos, L. Caro-Lara and R. Vicuña, *Environ. Microbiol. Rep.*, 2015, **7**, 388–394.
14 J. Li, Y. Wang, Y. Chen, Q. Xiong, J. Yang, L. Li and J. Li, *Chin. J. Chem. Eng.*, 2022, **49**, 170–177.
15 F. Trapani, A. Polyzoidis, S. Loebbecke and C. G. Piscopo, *Microporous Mesoporous Mater.*, 2016, **230**, 20–24.
16 H.-J. Li, L. Cheng, P. Sun, F.-F. Li and J. Qiu, *Water*, 2023, **15**, 878.
17 F. Fathieh, M. J. Kalmutzki, E. A. Kapustin, P. J. Waller, J. Yang and O. M. Yaghi, *Sci. Adv.*, 2018, **4**, 221.
18 B. Hunger, S. Matysik, M. Heuchel, E. Geidel and H. Toufar, *J. Therm. Anal.*, 1997, **49**, 553–565.
19 H. Kim, S. R. Rao, E. A. Kapustin, L. Zhao, S. Yang, O. M. Yaghi and E. N. Wang, *Nat. Commun.*, 2018, **9**, 1191.
20 J. K. Brennan, K. T. Thomson and K. E. Gubbins, *Langmuir*, 2002, **18**, 5438–5447.
21 J. Xu, T. Li, J. Chao, S. Wu, T. Yan, W. Li, B. Cao and R. Wang, *Angew Chem. Int. Ed. Engl.*, 2020, **59**, 5202–5210.
22 N. Hanikel, M. S. Prévot and O. M. Yaghi, *Nat. Nanotechnol.*, 2020, **15**, 348–355.
23 H. A. Almassad, R. I. Abaza, L. Siwwan, B. Al-Maythalony and K. E. Cordova, *Nat. Commun.*, 2022, **13**, 4873.
24 M. P. Silva, A. M. Ribeiro, C. G. Silva, G. Narin, I. B. Nogueira, U.-H. Lee, J. L. Faria, J. M. Loureiro, J.-S. Chang, A. E. Rodrigues and A. Ferreira, *Sep. Purif. Technol.*, 2020, **237**, 116336.

25 H. Kim, S. Yang, S. R. Rao, S. Narayanan, E. A. Kapustin, H. Furukawa, A. S. Umans, O. M. Yaghi and E. N. Wang, *Science*, 2017, **356**, 430–434.
26 Y. Tao, Q. Wu, C. Huang, W. Su, Y. Ying, D. Zhu and H. Li, *ACS Appl. Mater. Interfaces*, 2022, **14**, 10966–10975.
27 N. Hanikel, M. S. Prévot, F. Fathieh, E. A. Kapustin, H. Lyu, H. Wang, N. J. Diercks, T. G. Glover and O. M. Yaghi, *ACS Cent. Sci.*, 2019, **5**, 1699–1706.
28 Y. Tao, Q. Li, Q. Wu and H. Li, *Mater. Horiz.*, 2021, **8**, 1439–1445.
29 R. Sharma, G. Saab, M. Schoukens, T. R. van Assche and J. F. Denayer, *Appl. Mater. Today*, 2023, **35**, 101918.
30 J. Lord, A. Thomas, N. Treat, M. Forkin, R. Bain, P. Dulac, C. H. Behroozi, T. Mamutov, J. Fongheiser, N. Kobilansky, S. Washburn, C. Truesdell, C. Lee and P. H. Schmaelzle, *Nature*, 2021, **598**, 611–617.
31 M. Islamov, H. Babaei, R. Anderson, K. B. Sezginel, J. R. Long, A. J. H. McGaughey, D. A. Gomez-Gualdron and C. E. Wilmer, *npj Comput. Mater.*, 2023, **9**, 11.
32 Q. Li, Y. Ying, Y. Tao and H. Li, *Ind. Eng. Chem. Res.*, 2022, **61**, 1344–1354.
33 Z. Chen, Z. Shao, Y. Tang, F. Deng, S. Du and R. Wang, *ACS Mater. Au*, 2022, **3**(1), 43–54.
34 S. Chen, G. He, H. Hu, S. Jin, Y. Zhou, Y. He, S. He, F. Zhao and H. Hou, *Energy Environ. Sci.*, 2013, **6**, 2435.
35 Y. Kong, S. Zhang, Y. Gao, X. Cheng, W. Kong, Y. Qi, S. Wang, F. Yin, Z. Dai, Q. Yue and B. Gao, *J. Hazard. Mater.*, 2022, **423**, 127064.
36 R. Fan, N. Zheng and Z. Sun, *Energy Convers. Manag.*, 2022, **263**, 115693.
37 D. Fröhlich, E. Pantatosaki, P. D. Kolokathis, K. Markey, H. Reinsch, M. Baumgartner, M. A. van der Veen, D. E. De Vos, N. Stock, G. K. Papadopoulos, S. K. Henninger and C. Janiak, *J. Mater. Chem. A*, 2016, **4**, 11859–11869.
38 J. Zhang, H.-J. Bai, Q. Ren, H.-B. Luo, X.-M. Ren, Z.-F. Tian and S. Lu, *ACS Appl. Mater. Interfaces*, 2018, **10**, 28656–28663.
39 M. A. van der Veen, S. Canossa, M. Wahiduzzaman, G. Nenert, D. Frohlich, D. Rega, H. Reinsch, L. Shupletsov, K. Markey, D. E. de Vos, M. Bonn, N. Stock, G. Maurin and E. H. G. Backus, *Adv. Mater.*, 2023, e2210050.
40 Z. Zheng, H. L. Nguyen, N. Hanikel, K. K.-Y. Li, Z. Zhou, T. Ma and O. M. Yaghi, *Nat. Protoc.*, 2022, **18**, 136–156.
41 D. Lenzen, P. Bendix, H. Reinsch, D. Fröhlich, H. Kummer, M. Möllers, P. P. C. Hügenell, R. Gläser, S. Henninger and N. Stock, *Adv. Mater.*, 2018, **30**, 1705869.
42 K. S. Mertin, A. Mohtar, M. Bordonhos, M. L. Pinto, T. May, R. Herrmann and N. Stock, *Ind. Eng. Chem. Res.*, 2026, **65**, 7045–7055.
43 I. Jahan, T. H. Rupam, M. L. Palash, K. A. Rocky and B. B. Saha, *J. Mol. Liq.*, 2022, **345**, 117760.
44 G. Zahn, H. A. Schulze, J. Lippke, S. König, U. Sazama, M. Fröba and P. Behrens, *Microporous Mesoporous Mater.*, 2015, **203**, 186–194.
45 S. Zhang, J. Liu and L. Liu, *RSC Adv.*, 2021, **11**, 36928–36933.
46 H. Liu, M. Zhang, H. Zhao, Y. Jiang, G. Liu and J. Gao, *RSC Adv.*, 2020, **10**, 4045–4057.
47 W. T. Xie, Y. J. Dai, R. Z. Wang and K. Sumathy, *Renewable Sustainable Energy Rev.*, 2011, **15**, 2588–2606.
48 C. Gong, J. Lao, B. Wang, X. Li, G. Li, J. Gao, Y. Wan, X. Sun, R. Guo and J. Luo, *J. Mater. Chem. A*, 2020, **8**, 20162–20167.